The neural origins of shell structure and pattern in aquatic mollusks

Alistair Boettiger[a], Bard Ermentrout[b], and George Oster[a,1]

[a]Biophysics Graduate Group and Department of Molecular and Cellular Biology, University of California, 216 Wellman Hall, Berkeley, CA 94720; and [b]Department of Mathematics, University of Pittsburgh, 512 Thackeray, Pittsburgh, PA 15260

Edited by Eve Marder, Brandeis University, Waltham, MA, and approved February 13, 2009 (received for review October 20, 2008)

We present a model to explain how the neurosecretory system of aquatic mollusks generates their diversity of shell structures and pigmentation patterns. The anatomical and physiological basis of this model sets it apart from other models used to explain shape and pattern. The model reproduces most known shell shapes and patterns and accurately predicts how the pattern alters in response to environmental disruption and subsequent repair. Finally, we connect the model to a larger class of neural models.

neurosecretory | mathematical model | bifurcation

Seashells display a remarkable variety of ornate pigmentation patterns. Accumulating evidence now indicates clearly that shell growth and patterning are under neural control and that shell growth and pigmentation is a neurosecretory phenomenon. Most of this evidence has been gained by detailed studies of the mantle, a tongue-like protrusion of the mollusk that wraps around the edge of the shell and deposits new shell material and pigment at the shell's growing edge (see Fig. 1 *A* and *B*) (1, 2). The shell itself is composed of crystal structures of calcium carbonate interspersed with associated proteins and other organic compounds, some of which are pigmented and arrayed in intricate patterns (3, 4). This hard shell is covered by a thin organic layer of proteinaceous secretions, believed to function in regulating calcium crystallization (5). Early EM studies of the mantle recorded an extensive distribution of nerve fibers among the secretory cells (1, 6, 7). These fibers were later shown to have active synapses with secretory gland cells and synaptic inputs from other sensory organs in the mantle. From this evidence, it was proposed that neural-stimulated secretion controls shell growth (4, 7). The original evidence from gastropods has been extended to other mollusk taxa, including bivalves (8) and cephalopods, where improved experimental methods confirm clearly the role of neural control (9, 10). Neural recordings and neural cell ablation experiments have further verified the role of neural control in shell growth and repair (6, 11, 12).

This experimental data on mollusk shell construction and pigmentation allow us to formulate a new neural network model and develop a unified explanation for the generation of both shell shapes and patterns. Unlike the purely geometric representations proposed earlier to model shell shape (13–18), our model links shape generation directly to the dynamics of the underlying neural network. Recent experimental work describes how differential growth patterns can lead to shell-like structures (19–21) but does not explain the biological origin or mechanism of these growth patterns. The neural model presented here closes this gap by explaining how the mantle neural net can encode the appropriate information required for shell growth as well as pigment deposition.

Early attempts to reproduce shell patterns used cellular automata models, in which arbitrary rules determine the pigmentation of cells on a grid (22–24). Although they can reproduce some observed patterns, these models have shed little light on how such patterns actually arise in the animal. Inspired by the chemistry of diffusing morphogens, Meinhardt and coworkers (25–29) used a variety of different diffusion–reaction (DR) models to reproduce a wide variety of shell pigmentation patterns. Although no experimental evidence has been found for diffusing morphogens in patterning, the models can be viewed as an incomplete analogy for neural activity (chapter 12.4 in ref. 30).

Both the neural and DR models allow different ways of describing the phenomenon of local excitation with lateral inhibition (LALI). Ernst Mach (31) first described this phenomenon to explain the visual illusions now called "Mach Bands" and emphasized LALI's property of enhancing boundaries. Nearly a century later, Alan Turing (32) showed how LALI could be modeled by systems of nonlinear DR equations. This property was exploited by later workers, most notably Murray (30) and Meinhardt et al. (33–35) to model an extraordinary range of biological patterns. Indeed, DR models have become an all-purpose LALI metaphor in many domains wherein the underlying physics are clearly not diffusing substances (30, 36). All of these models exhibit spatial instabilities that lead to spatial patterns. The neural shell model presented here combines spatial with temporal instability because the mantle can sense previously laid patterns by, in a sense, looking backwards in time. Indeed, LALI in time is equivalent to a refractory period that leads to temporal oscillations. Meinhardt's DR models have succeeded in reproducing almost all of the patterns quite accurately, and we can hardly do better here. Our goal, however, is not to merely reproduce the patterns but to show how a single neural network model, based directly on the mantle anatomy, can capture all of the pattern complexity, as well as constructing the shell shape, and to relate the model to a broader class of experimentally observed neural network behavior.

Our exposition proceeds as follows. First we describe the neural net model as applied to the construction of the shell shape. We then proceed to define the most important classes of shell patterns and show how the model reproduces them. We also describe how the shell patterns respond to perturbations, such as injuries.

Results

A Neurosecretory Model of Shell Growth and Pattern Formation. Because we are interested only in the origin of shape and pattern and not the structural composition of the shell, we shall ignore the subsequent biomineralization that strengthens the shell distally from the leading edge. Secretions in the periostracal groove are controlled by the underlying neural network synapsing on the secretory cells. The activity of this neural network is stimulated by the existing pattern of shell deposition and pigment at the mantle edge. A schematic representation of this system is shown in Fig. 1*B*.

The shell is constructed by periodic—usually daily—bouts of secretion (40–42). These periodic increments are robust against many kinds of environmental variations (41). We model the secretions in daily steps, wherein the pattern of each day's layer of secretions, P_t, is a function of the preexisting layers, $P(t - \tau)$. We adopt the hypothesis of Bauchau (41) that the pigment pattern

Author contributions: G.O. designed research; A.B. performed research; B.E. contributed new reagents/analytic tools; A.B., B.E., and G.O. analyzed data; and A.B. wrote the paper.

The authors declare no conflict of interest.

This article is a PNAS Direct Submission.

[1]To whom correspondence should be addressed: E-mail: goster@nature.berkeley.edu.

This article contains supporting information online at www.pnas.org/cgi/content/full/0810311106/DCSupplemental.

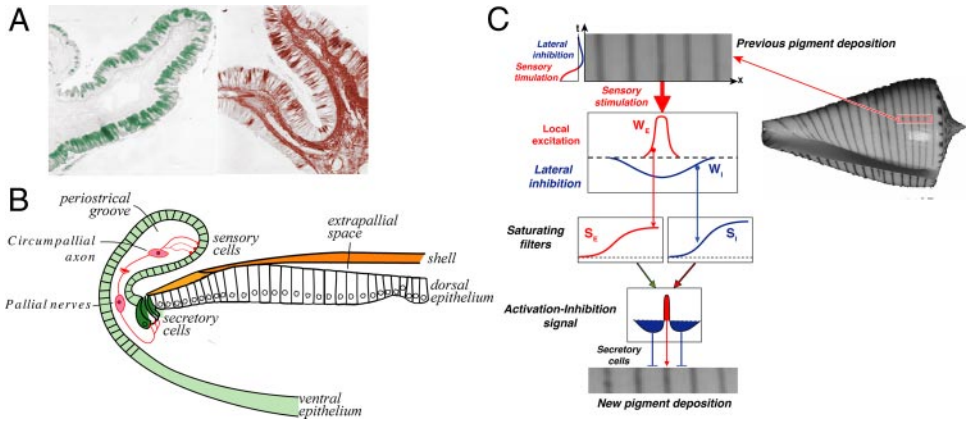

Fig. 1. Shell-making machinery. (*A*) EM of the mollusk mantle. The EM of a nautilus mantle is shown, with secretory epithelial cells stained green and nerve axons stained red. [Images reproduced with permission from ref. 10 (Copyright 2005, Wiley).] (*B*) Schematic representation of the mantle, showing the neurosensory cells, the circumpallial axons connecting these cells, and the neurons that control shell and pigment secretion. (*C*) Schematic illustration of the model. The existing edge pattern induces excitatory firing (red); the older, previous pattern is inhibitory (blue), indicated in the upper trace. For simulation purposes we use a Gaussian spatial kernel $W_{E,I} = \alpha_{E,I}\exp(-x^2/\sigma_{E,I}^2)$. Excitatory stimulation leads to sharp stimulation of the local region and weak inhibition of an even wider surrounding region. Neural stimuli are passed through saturating sigmoidal filters to determine the spatial pattern of activation or inhibition on the pigment secreting cells. We use $S_{E,I} = 1/[1 + \exp(\nu_{E,I}[\theta_{E,I} - K])]$, where K is the input from the spatial kernel. The pigment is then $P_{t+1} = S_E(W_E{\cdot}P_t) + S_I(W_E{\cdot}P_t) - R_t$, with $R_t = \gamma P_{t-1} + \delta R_{t-1}$ (see section A of *SI Appendix* for derivation, discussion, and alternate forms).

allows the mantle to position itself in register with the existing pattern. Fig. 1*C* shows a schematic diagram of how the model senses the pattern from previous days' secretions and lays down the current day's pattern.

The basic property of the neural net control of secretion lies in the phenomenon of LALI, common to many—if not all—neural networks. As we shall demonstrate, this general feature of neural nets will be sufficient to generate all of the observed shell patterns from a single mathematical model. A noteworthy aspect of this work is that LALI takes place both in space (along the mantle edge) and backwards in time (perpendicular to the mantle edge). A precise mathematical derivation of the model is given in *SI Appendix*, section A. Here we present an intuitive description.

Sensory organs in the mantle detect the presence of pigment and stimulate pigment secretion in local secretory cells. Consider a cell located at position x along the growing shell edge. The strength of its lateral stimulation of surrounding cells is represented by the curve, $W_E(x)$ (red trace in Fig. 1*C*). The same sensory input excites a wider inhibitory field in the mantle, which we describe by the curve, $W_I(x)$ (blue trace in Fig. 1*C*). Because the mantle wraps around the top edge of the shell, it senses, in addition to the exposed edge, some previous history of pigmentation a distance τ back from the leading edge. Pigmentation near the leading edge has an excitatory effect on local secretion, whereas pigmentation sensed further from the edge has an inhibitory effect. We incorporate this effect into the excitatory and inhibitory kernels by making them functions of τ and integrating back in time (i.e., distance from the shell edge). Only the qualitative features of the functions W_E and W_I, not their precise shape, are important for the pattern. For computational analysis, we represent the excitation and inhibition functions with Gaussian curves of different widths and different relative amplitudes (43).

Neurons have a nonlinear, saturating response to their net stimulation (44, 45). There is a characteristic threshold for the neuron, around which it is most sensitive to changes in the stimulation rate. Once the stimulation exceeds this threshold, the rate of change in activity in response to change in stimulation saturates. In general, the characteristics of this sigmoid input–output response curve will be different for inhibitory and excitatory synapses. Therefore we subject the excitation and inhibition to separate saturating input–output functions S_E (Fig. 1C, red) and S_I (Fig. 1*C*, blue). This step filters the sensory input that stimulates the secretory cells.

The secretion of pigment in the current layer, P_t, is determined by the net stimulation of the secretory cells. Because of lateral inhibition in the τ direction, the current secretion is affected both directly and indirectly by the previous pattern. The pigmented portion of these depositions provides "markers" and allows us to see how this sensory network propagates the pattern from layer to layer over time.

The model can be cast in several nearly equivalent mathematical forms; these forms are presented in *SI Appendix*, section A. The specific analytical forms of the kernels representing the lateral connections and the saturation functions representing the nonlinear neural input–output responses do not affect the patterns generated by the model.

Explaining Shell Structure. The location and shape of the initial shell secretions are determined during embryonic morphogenesis. After the initial shell secretion, the mollusk constructs the rest of the shell enclosure, regularly expanding the enclosure to accommodate its growth. In gastropods (snails), the shell grows outward and spirals downward from the original region of shell secretion by successively adding small increments of additional shell material to the leading edge. A variety of mathematical representations of the final geometry have been proposed, (see *SI Appendix*, section C) (13, 16, 29,

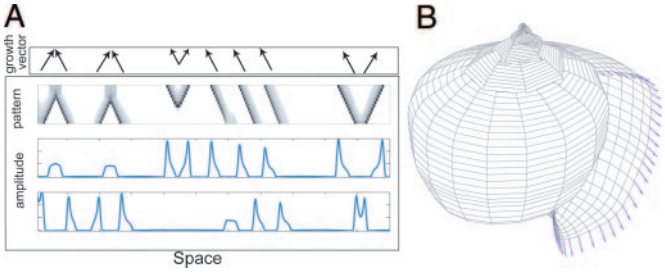

Fig. 2. Explaining structure. (*A*) The neural model explains how the aperture-growth vectors arise from the neural architecture in the mantle. The bottom plots show neural excitation at 2 different times (4 days apart). The effective growth vectors resulting from this pattern of excitation is shown at the top. (*B*) Aperture-growth vectors generated by the model to create spiral-shaped gastropods.

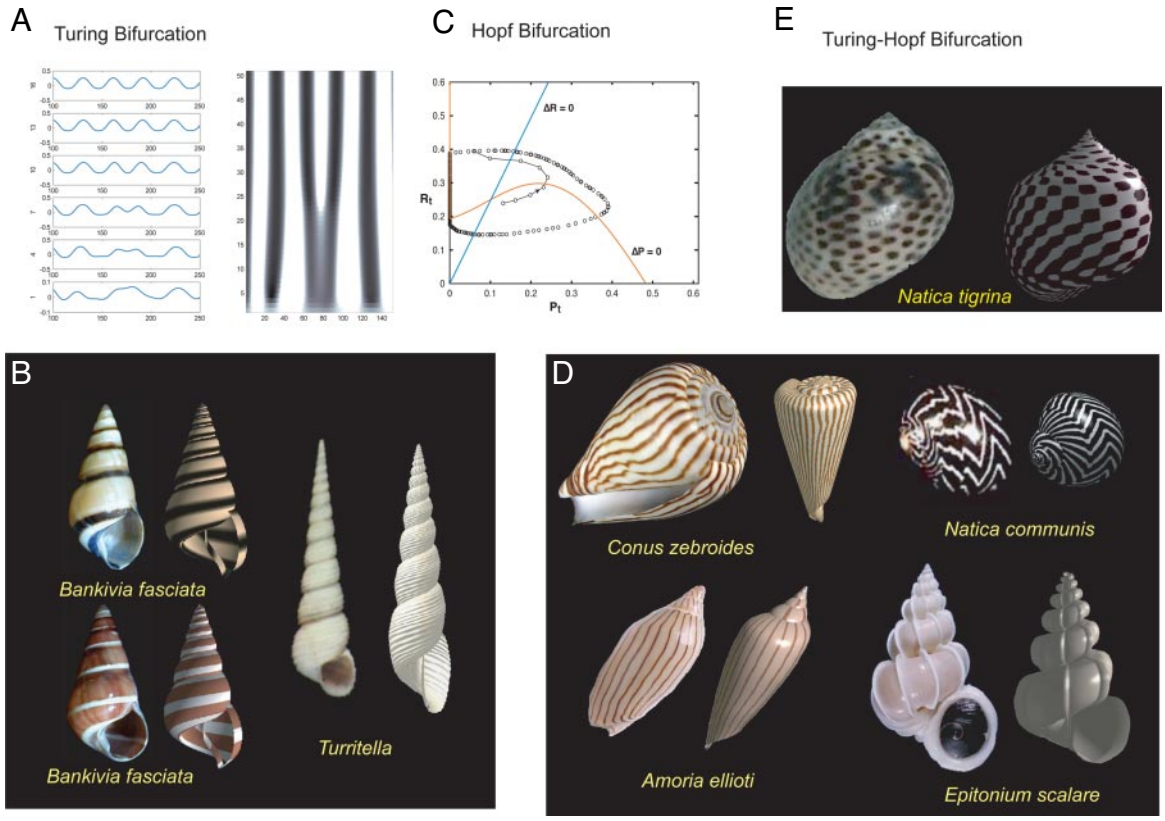

Fig. 3. Simple bifurcation patterns. In all images, the real shell is shown on the left, and the simulated shell on the right. (*A*) The gradual stabilization from random noise (*Bottom*) into periodic stripes (*Top*) shows how Turing instabilities give rise to patterns of stable bands perpendicular to the growing shell edge. Note that activation centers separate and shift as each one carves out a domain of influence. (*B*) Turing patterns. *B. fasciata* exhibits Turing bands of pigment, and *Turritella* exhibits structural ridge bands. (*C*) Phase plot of model variables shows the periodic orbits of a limit cycle created by a Hopf bifurcation. (*D*) Patterns of periodic stripes. This periodic activity may influence secretion of structural elements instead of pigment, resulting in the periodic flanges seen on *E. scalare*. The zigzag stripes shown on *N. communis* were generated by a combination of Hopf bifurcation with wave generation as described in Fig. 4. (*E*) Hopf bifurcations and Turing instabilities can occur simultaneously, leading to patterns like that of *N. tigrina*.

46). The underlying phenomena that generate this spiral growth pattern are unspecified, as are the differences between species that account for the different spirals—or no spiral at all, as in the bivalves. Rice (19) provided some of the first insights into these questions. This work was extended to growth vector models which demonstrated that many different coiled shell forms could be reproduced by varying secretion rates appropriately around the aperture (as shown in Fig. 2*B*) (20, 21).

We propose that neural activity controls the amount and direction in which shell material is secreted. The neural activity along the mantle determines the local secretion rate and, thus, the angle and magnitude of the growth vectors, as illustrated in Fig. 2*A*. The central point here is that the same model that generates the patterns can generate the shell geometry as well. In the discussion to follow, we shall augment the pigment patterns generated by the model with a few examples of shell growth generated by the same model. The dynamics of shell growth are best appreciated as movies computed from the neural secretion model, a frame of which is shown in Fig. 2*B*. Examples are given in Movie S1 and Movie S2.

Understanding Pigmentation Patterns. The neural architecture of local excitation and long-range inhibition gives rise to a broad array of stable patterns. The type of pattern depends on the relative ranges and strengths of the interactions and the steepness and thresholds of the firing response curves. Remarkably, all of the patterns initiate from 3 basic mathematical phenomena arising from the LALI property: spatial instabilities (Turing bifurcations), temporal instabilities (Hopf bifurcations), and traveling waves*. Analytical demonstrations of these instabilities are presented in *SI Appendix*, section B.

Bifurcations Create Periodic Patterns in Space and Time. LALI readily gives rise to patterns of parallel stripes orthogonal to the shell's leading edge. This development takes place because the spatially uniform state is unstable to small, random perturbations or slight heterogeneities in the neural network (i.e., a Turing instability) (30, 47). Briefly, the process works in the following manner. A slightly more active local group of cells exerts a stronger inhibitory effect on its neighbors. This lateral inhibition weakens the activity in the neighbors and consequently weakens the inhibitory effect they exert on the original population; this weakening of the neighbor population causes the activity of the original group of cells to increase. At the same time, the activity reduction in the neighbor cluster allows the next cluster over to increase its activity because its inhibition is lowered. The result is a standing wave of neural activity that deposits stable pigmentation stripes normal to the aperture. The width of the stripes reflects the extent of the excitatory region in the mantle and the width of the gaps reflects the extent of the inhibitory connections. Some examples are shown in Fig. 3*D*.

If we increase the strength of the stimulation arising from the previous day's pattern (i.e., the amplitude of the activation kernel

*The waves probably originate from an infinite dimensional saddle-node bifurcation, but we have not proven this here.

Fig. 4. Wave patterns. (*A*) Patterns formed by traveling waves of excitation. Asymmetric regions of excitation travel toward the stronger side, as illustrated by C. clerii in B. When these waves collide, they may reflect, as shown in this simulation and on the shells of *C. clerii* and *C. marblus*. The waves may annihilate, as shown on the shells of *Conus viceweei*. A wave may also emit ''reverse'' waves, creating the beautiful tent patterns of *Olivia porphyria*. (*B*) Graphs of neural activity across the leading edge and close-up of resulting secretions for select shells. (*C*) Some traveling waves of excitation leave excited regions behind as they cross the mantle. At a critical width, the cumulative inhibition shuts down signaling, creating a region devoid of pigment. This region is slowly reclaimed by waves traveling back into it, as shown in the simulation of *C. innexa* and *C. marblus* in *B* and *C*. (*D*) Some of the diverse patterns produced by the model by combinations of wave collisions and emissions.

in the τ direction), the pattern can switch to alternating bands parallel to the shell edge, as shown in Fig. 3*E*. To create these periodic patterns, secretion-stimulating neurons must cycle between successive periods of stimulation and quiescence. A plot of the current pigmentation versus the past pigmentation (i.e., a phase plane portrait) will trace out a single loop around which the system continuously cycles (see Fig. 3*C*). Such periodic orbits on the phase plane (limit cycles) arise from parameter changes triggering so-called Hopf bifurcations, which are well-known in models of repetitively firing and bursting neurons (45). These periodic instabilities can arise in several ways. For example, when there are different thresholds for excitatory and inhibitory signals, the neural network may be excitable at low-pigment-induced stimulation but inhibitory under strong activity. A low basal level activity in the absence of signaling triggers a slow, positive feedback, which gradually amplifies the signal and eventually triggers the high-threshold inhibitory response, which shuts neuronal firing back down to its basal level, from which the process begins again. This process leads to stable cycles of oscillation, which produce periodic bands of pigment parallel to the growing edge of the shell, whose period can be many multiples of the secretory period (e.g., 1 day). Excitatory lateral connections tend to synchronize the population into parallel bands like those seen on shells of *Amoria ellioti*. Stronger lateral inhibition induces the patterns to lag each other, forming instead periodically distributed zigzag patterns, like those of *Natica communis*. For a mathematical derivation of synchronizing phenomena among neural limit cycle oscillators, see ref. 45. Finally, Hopf bifurcations may coincide with a Turing instability, leading to patterns periodic in both space and time, like the checkerboard patterns of *Natica tigrina* shown in Fig. 3*B*.

In Fig. 3 *D* and *E*, we show how network-induced secretion of shell material, instead of pigment, leads to the growth of the shell geometry in *Turritella* and *Epitonium scalare*.

Asymmetric Activity Creates Traveling Waves. Traveling waves of pigmentation arise when previous firing activity represses future firing activity while exciting lateral activity. An asymmetric region of activation (as in the wedge shape in Fig. 4*A*) induces stronger stimulation toward its high side than toward its tail. This uneven lateral excitation induces the pigment in the next layer to spread laterally in front of the wedge. The repression from having fired narrows down the tail, and the whole wedge shifts sideways toward the high side. Successive depositions thus create a traveling line of pigment at an oblique angle to the shell edge. When two such waves of pigmentation collide, they may mutually annihilate (as in *Conus clerii*), singularly annihilate (as *Conus vicweei*), or reflect (*Tapes litarus*) (Figs. 4 and 5*E*). Close examination of reflecting waves show that each wave is actually quenched but then reignites because the activation width is broader than the inhibition region.

Depending on the size and shape of the kernels, when waves approach each other they can either slow down or speed up. Thus, regular reflecting waves can create patterns of spots as on *Natica stercusmucarum* (*SI Appendix*, section H) or teardrops like on *Conus marblus* (Fig. 4*A*), depending on how the overlapping excitation and inhibition kernels either accelerate or decelerate approaching and separating waves. If the previous firing repression

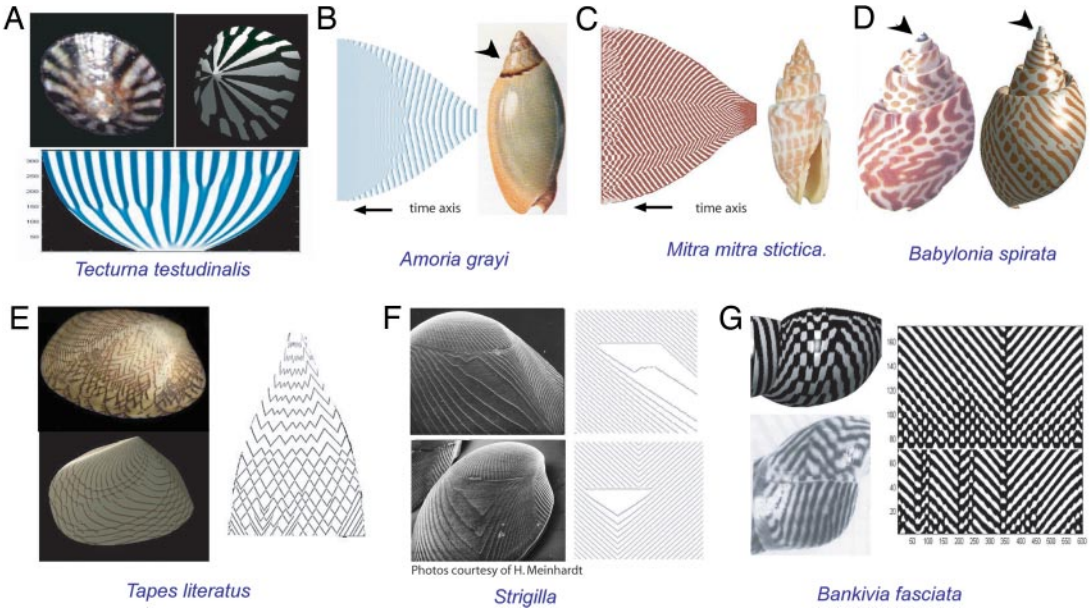

Fig. 5. The effects on patterns of shell growth and perturbations. As the shell grows, the width of the pattern domain increases leading to changes in the pattern. (*A–E*) These patterns include line bifurcations of *T. testudinalis* (*A*), collapse of oscillations in *Amoria grayi* (*B*), destabilization of waves into patchy dots on *M. mitra stictica* (*C*), emergence of a pattern from a uniform field in *Babylonia spirita* (*D*), and transition from annihilating to reflecting waves on *T. litarus* (*E*). Patterns change in response to scratches, which remove information about the previous pattern. (*F*) Traveling waves in *Strigilla* shells slow down and deflect away from the growing edge. [Photo adapted and reproduced with permission from ref. 27 (Copyright 1987, Elsevier.)] (*G*) *B. fasciata* goes through repeated stabilizations from dots to stripes. Shells in *B–D* are from ref. 52.

activity has a high threshold, waves traveling apart remain connected at the tails until the stimulation abruptly crosses the threshold and all pigmentation stimulation shuts off abruptly. The still-stimulated edges, however, travel back into the unpigmented region, leaving a triangular gap devoid of pigment. This gap is seen on many shells (e.g., *Conus bullatus* and *Conus thailandis*, seen in Fig. 4*C*). Fig. 4*B* also shows the detailed steps that lead to the fractal-like triangles of *Cymbiola innexa* in Fig. 4*C*. Additional patterns generated by the model are shown in Fig. 4*D* and in *SI Appendix*, section H.

Effects of Shape and Environment on Patterns. The pigmentation patterns on many shells change qualitatively as a result of shell growth or environmental disruption. Our simple neural model provides a mechanistic explanation for many of these pattern changes.

The length scale of the pattern is determined by the distribution of axon and dendrite lengths. As the animal grows and more neurons incorporate into the mantle, existing patterns may become unstable. Parallel lines perpendicular to the shell edge may widen or bifurcate as the overlap between lateral inhibition decreases. Both effects are apparent in the limpet *Tectura testudinalis* in Fig. 5*A*. Another common observation is that patterns of pigmentation are homogeneous on small domains (relative to the average neuronal connection range). This observation explains why many shells start with either no pigment or uniform pigment and develop intricate patterns only after the mantle edge grows to the appropriate length. An example is the shell of *Babylonia spirata* in Fig. 5*D*. Note the lack of pigmentation in the small twists that form the top of the spiral. In contrast, regular patterns, such as oscillating bands, are stable only when the domain size is small. As the domain becomes large, synchrony across the mantle is lost and the pattern degenerates into a uniform pigmentation as seen on the shells of *Amoria grayi* (shown in Fig. 5*B*). Additionally, loss of pattern synchrony may cause the pattern to degenerate from alternating bands into a mesh of dots, as the domain becomes too large to maintain global synchrony in the presence of small background noise. This effect is seen on a variety of shells, including the *Mitra mitra stictica* shells shown in Fig. 5*C*. Other pattern bifurcations are also captured by the model. The bivalve *T. litarus* exhibits regular traveling waves across its shell. Near the top of the shell these waves collide and terminate in V-shaped patterns. However, as the domain size increases, the waves become reflecting, bifurcating in shaped intersections when they collide (Fig. 5*E*).

In addition to predicting how patterns are created ab initio, the model predicts how the system responds to perturbations in the pattern. Ablation of a small portion of the ridge pattern on a *Strigilla* shell allows for spontaneous activation of new waves (manifested by the V's formed) and acceleration of existing waves, as evidenced in the lines becoming more closely parallel to the growing edge. Simulations of pattern ablation capture both of these effects, which appear in a field of traveling waves and at an annihilation point, as shown in Fig. 5*F*. *Bankivia fasciata* synchronize in steps from random initiation provided by variable background rates. First a mesh-like pattern of dots emerges; these dots subsequently synchronize into uniform bands as explained above. If the pattern is disrupted by an injury, the pattern restabilizes from dots to stripes again, a property readily illustrated by the model in Fig. 5*G*.

Insights into Mollusk Evolution. An attractive feature of the neuronal model is its suggestive mechanism for the evolution of the observed pattern diversity. Because very similar species can exhibit significantly different patterns, the pattern difference cannot be the result of dramatic anatomical differences. The neural model provides a common mechanism whereby small changes in the parameters lead to large changes in the patterns. The model also makes testable predictions about which sets of patterns one is likely to find within a genus and which sets of patterns are not likely to occur together in a genus. Our model predicts a greater evolutionary separation would be required. Surprisingly, some of the dramatically differently patterned species of cone shells can be reasonably well-reproduced by parameter sets that are quite close to each other, as shown in *SI Appendix*, section H and Fig. S5.

Discussion

In this work, we have shown that a single neurosecretory model can replicate both the growth of mollusk shells and the enormous diversity of pigment patterns they exhibit. The model is built around the general property of local excitation coupled with lateral inhibition common to most neural networks. A noteworthy feature in this model is that the same network architecture operates in both the spatial and time directions because the pigment patterns develop sequentially as the mantle lays down periodic increments of shell and pigment. Thus, the shell pattern records the complete time history of its neurosecretory activity. One might think of the pattern as an electroencephalogram, or the history of the thoughts of a mollusk! In general, waves propagating through a 3-dimensional neural network (e.g., a cortical column) have this same property: Local excitation/lateral inhibition extends laterally, as well as backwards in space from where the excitation came, which is essentially backwards in time.

By exploiting the permanent record of neural activity that mollusks have incorporated into their shells, we have achieved a mechanistic understanding of how these diverse, and seemingly very different, patterns arise. We have shown that all of the patterns emerge from combinations of 3 types of bifurcations: Turing and Hopf bifurcations, wave propagation, and collisions, which probably originate in saddle-node bifurcations. The intuitions we have developed in the study of mollusk shells may provide a useful foundation for studying other types of neural patterns, such as the dynamic patterning of cuttlefish skin controlled by a neuromuscular network that exposes and hides chromatophores. We have found that the mollusk model can reproduce many patterns observed in the cuttlefish mantle (see *SI Appendix*, section E) that form sequentially as a wave. The cuttlefish patterns change much faster than the mollusk patterns, but their origin is fundamentally the same: Both are products of neural net activity. Insights from the study of complex visible neural patterns like these may prove useful in understanding normally invisible patterns of neural activity, such as the structured spatial organization of neural activity distributed over the mammalian cortex. Here we have seen that the mollusk waves slow down and reflect in a manner similar to that observed in cortical waves (48). Such wave collisions might allow for comparison of cortical predictions with sensory input: Annihilation occurs when waves are identical and an error wave propagates out when they are different.

Our mechanistic explanation of how a neural system determines the future pattern from the previous pattern suggests an interesting parallel with other cortical processes. It is not entirely unlike the challenge the brain addresses of predicting the future from its internal neurological model of the world. Most theories of this process make analogies to Bayesian inference (49–51). Our work suggests how these models may be recast in terms of physiological neural parameters that may underlie such Bayesian prediction models (see *SI Appendix*, section F). We suspect many new insights await in the study of spatial patterns of neural activity.

Materials and Methods.

The model was simulated and results plotted as graphics in MATLAB 2007b.

ACKNOWLEDGMENTS. We thank B. Westermann and H. Meinhardt for permission to reproduce the noted images in Figure 1*A* and Figure 5*F*. A.B. and G.O. were supported by National Science Foundation Grant 0414039. B.E. was supported by the National Science Foundation Division of Mathematical Sciences. A.B. was supported by National Institute of Biomedical Imaging and Bioengineering Training Grant in Physical Biosciences T32 EB005586-01A2.

1. Saleuddin ASM, Dillaman RM (1976) Direct innervation of the mantle edge gland by neurosecretory axons in helisoma duryi (Mollusca: Pulmonata). *Cell Tissue Res* 171:397–401.
2. Saleuddin A, Kunigelis S, Khan H, Jones G (1980) Possible control mechanisms in mineralization in Helisoma duryi (mollusca: pulmonata). *The Mechanisms of Biomineralization in Animals and Plants* eds Omori M, Watabe N (Tokai Univ Press, Tokyo).
3. Checa AG, Okamoto T, Ramírez J (2006) Organization pattern of nacre in *Pteriidae* (*Bivalvia: Mollusca*) explained by crystal competition. *Proc R Soc London Ser B* 273:1329–1337.
4. Saleuddin ASM (1979) *Pathways in Malacology* (Junk, The Hague), pp 47–81.
5. Taylor JD, Kennedy WJ (1969) The influence of the periostracum on the shell structure of bivalve molluscs. *Calcif Tissue Int* 3:274–283.
6. Dillaman RM, Saleuddin ASM, Jones GM (1976) Neurosecretion and shell regeneration in *Helisoma duryi*. *Can J Zool* 54:1771–1778.
7. Saleuddin ASM, Kunigelis SC (1984) Neuroendocrine control mechanisms in shell formation. *Am Zool* 24:911–916.
8. Saleuddin A (1974) An electron microscopic study of the formation and structure of the periostracum in *Astarte* (*Bivalvia*). *Can J Zool* 52:1463–1471.
9. Westermann B, Beurelein K, Hempelmann G, Shipp R (2002) Localization of putative neurotransmitters in the mantle and siphuncle of the mollusc *Nautilus pompilius*. *Histochem J* 34:435–440.
10. Westermann B, Schmidtberg H, Beurelein K (2005) Mantle organization of *Nautilus pompilius*. *J Morphol* 264:277–285.
11. Dogterom AA, van Loenhout H, van der Schors RC (1979) The effects of growth hormone of *Lymnaea* stagnalis on shell calcification. *Gen Comp Endocrinol* 39:63–68.
12. Wilbur K, Saleuddin ASM (1983) *The Mollusca* (Academic, New York).
13. Thompson DW (1952) *On Growth and Form* (Cambridge Univ Press, Cambridge, UK).
14. Raup D (1961) The geometry of coiling in gastropods. *Proc Nat Acad Sci USA* 47:602–629.
15. Raup D (1962) Computer as aid in describing form in gastropod shells. *Science* 138:150–152.
16. Raup D (1965) Theoretical morphology of the coiled shell. *Science* 147:1294–1295.
17. Raup D (1966) Geometric analysis of shell coiling: General problems. *J Paleontol* 40:1178–1190.
18. Raup DM (1969) Modeling and simulation of morphology by computer. *Proc N Am Paleontol Conv B* 71–83.
19. Rice S (1998) The bio-geometry of mollusc shells. *Paleobiology* 24:133–149.
20. Hammer O, Bucher H (2005) Models for the morphogenesis of the molluscan shell. *Lethaia* 38:111–122.
21. Ubukata T (2005) Theoretical morphology of bivalve shell sculptures. *Paleobiology* 31:643–655.
22. Waddington CH, Cowe J (1969) Computer simulations of a molluscan pigmentation pattern. *J Theor Biol* 25:219–225.
23. Kusch I, Markus M (1996) Mollusc shell pigmentation: Cellular automaton simulations and evidence for undecidability. *J Theor Biol* 178:333–340.
24. Wolfram S (1984) Cellular automata as models of complexity. *Nature* 311:419–424.
25. Meinhardt H (1984) Models for positional signalling, the threefold subdivision of segments and the pigmentation pattern of molluscs. *J Embryol Exp Morphol* 83(Suppl):289–311.
26. Meinhardt H, Klingler M (1986) Pattern formation by coupled oscillations: The pigmentation patterns on the shells of molluscs. *Lecture Notes in Biomathematics* (Springer, Berlin), Vol 7.
27. Meinhardt H, Klingler M (1987) A model for pattern formation on shells of molluscs. *J Theor Biol* 126:63–89.
28. Meinhardt H, Prusinkiewicz P, Fowler D (2003) *The Algorithmic Beauty of Sea Shells* (Springer, New York), 3rd Ed.
29. Fowler DR, Meinhardt H, Prusinkiewicz P (1992) Modeling seashells. *Comput Graphics* 26:379–387.
30. Murray JD (2003) *Mathematical Biology* (Springer, New York), 3rd Ed, pp 638–655.
31. Mach E (1865) On the effect of the spatial distribution of light stimulus on the retina, I. *Sitzungsber Math Nat Klasse Kaiserl Akad Wiss* 52:303–332.
32. Turing A (1952) The chemical basis of morphogenesis. *Philos Trans R Soc Ser B* 237:37–72.
33. Gierer A, Meinhardt H (1972) A theory of biological pattern formation. *Kybernetik* 12:30–39.
34. Meinhardt H (1982) *Models of Biological Pattern Formation* (Academic, New York).
35. Meinhardt H, Gierer A (2000) Pattern formation by local self-activation and lateral inhibition. *BioEssays* 22:753–760.
36. Winfree A (2001) *The Geometry of Biological Time* (Springer, Berlin), 2nd Ed.
37. Amari S-I (1977) Dynamics of pattern formation in lateral-inhibition type neural field. *Biol Cybern* 27:77–87.
38. Ellias S, Grossberg S (1975) Pattern formation, contrast control, and oscillations in the short term memory of shunting on-center off-surround networks. *Biol Cybern* 20:69–98.
39. Wilson H, Cowan J (1973) A mathematical theory of the functional dynamics of cortical and thalamic nervous tissue. *Kybernetik* 13:55–80.
40. Berard H, Bourget E, Frechette M (1992) Mollusk shell growth: External microgrowth ridge formation is uncoupled to environmental factors in *Mytilus edulis*. *Can J Fish Aquat Sci* 49:1163–1170.
41. Bauchau V (2001) Developmental stability as the primary function of the pigmentation patterns in bivalve shells? *Belg J Zool* 131(Suppl 2):23–28.
42. Lutz RA, Rhoads DC (1980) *Skeletal growth of aquatic organisms; Biological records of environmental changes* (Plenum, New York), pp 203–254.
43. Dayan P, Abbott LF (2001) *Theoretical neuroscience: Computational and mathematical modeling of neural systems* (MIT Press, Cambridge, MA), pp 62.
44. Cowan JD (1968) *Neural Networks* (Springer, Berlin), pp 181–188.
45. Ermentrout B (1998) Neural networks as spatio-temporal pattern-forming systems. *Rep Prog Phys* 61:353–430.
46. Checa A (2002) Fabricational morphology of oblique ribs in bivalves. *J Morphol* 254:195–209.
47. Oster G (1988) Lateral inhibition models of developmental processes. *Math Biosci* 90:265–286.
48. Xu W, Huang X, Takagaki K, Wu J-Y (2007) Compression and reflection of visually evoked cortical waves. *Neuron* 55:119–129.
49. Knill DC, Pouget A (2004) The Bayesian brain: The role of uncertainty in neural coding and computation. *Trends Neurosci* 27:712–719.
50. Doya K, Ishii S, Pouget A, Rajesh PNR, eds (2007) *The Bayesian Brain: Probabilistic Approaches to Neural Coding* (MIT Press, Cambridge, MA).
51. Huang G (2008) Is this a unified theory of the brain? *New Sci* 2658:30–33.
52. Oliver APH, Nicholls J (1975) *The Larousse Guide to Shells of the World* (Larousse, New York).